Molecular dynamics simulations of *a*-SiC films

V. I. Ivashchenko,[1] P. E. A. Turchi,[2] V. I. Shevchenko,[1] and O. A. Shramko[1]
[1]*Institute of Problems of Materials Science, NAS of Ukraine, Krzhyzhanovsky Street 3, 03142 Kyiv, Ukraine*
[2]*Lawrence Livermore National Laboratory, L-353, P.O. Box 808, Livermore, California 94551, USA*
(Received 5 March 2004; revised manuscript received 25 May 2004; published 7 September 2004)

Empirical molecular dynamics simulations combined with a recursion procedure are applied to the study of the atomic and electronic structures of *a*-SiC thin films. The films are generated from the condensation of diluted Si-C vapor on a crystalline silicon substrate similarly to atom-by-atom deposition. The as-deposited films are annealed at different temperatures. Growth kinetics, bonding configuration, chemical ordering, cohesion, relaxation effects, surface roughness, atomic level stress, and electronic properties of the films are investigated as functions of the deposition parameters: vapor temperature, applied particle force, and substrate and annealing temperatures. The results are compared with those associated with bulk and film samples of *a* -SiC generated from the melt. The main theoretical findings on *a*-SiC films are in rather good agreement with experimental evidences.

DOI: 10.1103/PhysRevB.70.115201 PACS number(s): 61.43.Dq, 71.15.Pd, 71.23.Cq

I. INTRODUCTION

Recent progress made in chemical vapor deposition (CVD), mainly plasma enhanced-CVD (PECVD), of hydrogenated amorphous silicon carbide (*a*-SiC:H) films holds promise for producing semiconductor devices.[1–4] The optoelectronic and microstructural properties of such films have been widely studied.[2–9] However, in recent years, there has been growing interest in preparing unhydrogenated amorphous silicon carbide films (*a*-SiC) by using various techniques such as laser-ablation deposition (LAD), pulsed laser deposition, triode-sputtering deposition, rf, and dc magnetron sputtering, and arc deposition.[10–18] Numerous studies have also reported that *a*-SiC layers can be produced under high-energy particles (electron, neutron, or ions) bombardment of crystalline silicon carbide.[19,20] This interest has been primarily motivated by the unique tribological properties of hydrogen-free films. Unhydrogenated amorphous SiC layers were shown to exhibit mechanical properties that are superior to those of their hydrogenated counterparts. In particular, Khakani *et al.*[10,11] and Cros *et al.*[12] have reported that LAD *a*-SiC has hardness and Young's modulus of about 30–52 GPa and 242–400 GPa, respectively, almost twice as high as that of PECVD *a*-SiC:H. The abrasive wear resistance of arc-deposited *a*-SiC coatings was found to be several times higher than that of silicon wafers.[13] Several experimental investigations also show that the properties and growth kinetics of *a*-SiC and *a*-SiC:H layers drastically depend on the deposition technique and parameters.

Hydrogen-free bulk silicon carbide was investigated theoretically in the framework of a first-principles pseudopotential approach (PA)-molecular dynamics (MD) (Refs. 21 and 22) and tight binding (TB)-MD simulations.[23,24] In addition empirical potential (EP)-Monte Carlo (MC) simulations,[25–28] EP-MD simulations[19,20,29–31] were used to study the atomic configurations and chemical ordering. The atomic and electronic structures of *a*-SiC:H were investigated with the help of the PA-MD (Ref. 32) and TB-MD (Ref. 33) simulations. Most *a*-SiC samples were generated by cooling the high-temperature 3C-SiC melt.[21,22,25–31] Both the TB 128-atom unhydrogenated and hydrogenated samples were obtained from the diluted Si-C (Refs. 23 and 24) and Si-C-H vapors.[33] A different approach was used in Refs. 34–37 to generate *a* -SiC. The authors[34–37] have employed empirical MD simulations of displacement cascades under ion irradiation to study atomic arrangements in *a*-SiC. All the computational schemes mentioned above give similar sample characteristics. The main difference lies in the evaluation of the extent of the chemical ordering. The structures with low chemical ordering were generated by using PA-MD and TB-MD simulations,[21,23,24] whereas *a*-SiC samples with comparatively high chemical ordering were prepared by using techniques based on the empirical Tersoff potential.[19,20,25–31,34–37] In contrast to the bulk *a*-SiC that has been widely studied with various theoretical and experimental procedures, no theoretical investigation of *a*-SiC films grown on a silicon substrate was yet carried out.

To fill this gap, we have generated a series of theoretical samples representing condensed *a*-SiC thin films on a silicon slab. For this purpose, an atom-by-atom deposition scheme based on large-scale EP-MD simulations was proposed. Our motivation was based on the following facts. For various applications *a*-SiC (*a*-SiC:H) films are usually grown by vapor-growth or sputtering techniques, and it is rather difficult to prepare them from the liquid phase using rapid quenching. Besides, the samples generated from the liquid phase do not contain voids, which are present in *a*-SiC films in large quantities. Therefore, instead of accounting for all the peculiarities of an experimental deposition, which is challenging, we tried to single out some of the main features of such a process. A series of *a*-SiC films were generated from a diluted vapor by means of vapor condensation on a substrate of crystalline silicon under various deposition conditions. The selected controlled deposition parameters were: vapor temperature, normally applied particle force, and substrate temperature, and the growth kinetics was analyzed as a function of these parameters. To investigate the effect of annealing on film properties one of the as-deposited samples

was annealed at various temperatures. The atomic and electronic characteristics of the samples were thoroughly studied. In addition, for comparison purpose, bulk and film *a*-SiC samples were generated by using a more traditional approach, i.e., by cooling the 3C-SiC melt. The simulated film characteristics are compared with those obtained experimentally and theoretically on film and bulk *a*-SiC samples whenever possible. In the absence of published results, our findings will be compared with those established for *a*-SiC:H films.

The paper is organized as follows: In Sec. II we describe the peculiarities of the EP-MD simulations, and introduce the recursion procedure for computing the densities of states (DOS). Section III is devoted to the results of the study of the influence of the deposition parameters (vapor temperature, applied force, and substrate temperature) on film characteristics. The results on film annealing and DOS investigations are also presented in this section. Finally, the main conclusions are given in Sec. IV.

II. COMPUTATIONAL APPROACH

A sample consisting of 1344 atoms, i.e., 768 Si atoms belonging to a substrate and 576 atoms with an equal number of Si and C atoms belonging to SiC vapor in a $21.72 \times 21.72 \times 200.0$ Å rectangular cell is initially considered for MD simulations. The periodic boundary conditions along the *x*- and *y*-directions are taken into account. No periodic condition is imposed to the cell in the *z*-direction. The film condensation is carried out with EP-MD simulations, in the constant number of particles-volume-temperature (NVT) ensemble, based on the Tersoff potential for SiC (Ref. 27) that does not take the sp^2 C-C interaction into account. The simulation cell contains a substrate representing the lower (001) silicon slab having the $(4\times4\times6)$ a_0 configuration (a_0 is the lattice parameter of *c*-Si), and an upper reservoir with the SiC diluted vapor. The vapor reservoir is thermostated to maintain the vapor at a specific temperature. It is displaced relatively to the substrate along the *z*-direction by a distance that exceeds the film thickness. A normal force directed towards the substrate is applied to each atom in the reservoir. The system is immovable due to the fixed lower substrate layer. The next six layers of the substrate are thermostated to control the substrate temperature. The controlled deposition parameters are: the vapor temperature (T_G), the normally applied particle force (F_N), and the substrate temperature (T_S). Each deposition is carried out during 18, 20, and 22 ps, and after complete deposition a small amount of isolated atoms is found. Such an approach allows us to evaluate the average film condensation rate (film growth rate). Prior to deposition, the vapor and the substrate are equilibrated at T_G and T_S, respectively, for 5 ps. We have investigated the as-deposited films, i.e., the films that were not equilibrated after the deposition, and the relaxed samples that were equilibrated at temperatures equal to T_S during 50 ps and further cooled down to 300 K and equilibrated for 5 ps. Also, one sample was annealed at $T_a = 600$, 1300, 2000, and 2500 K using both the NVT and NPT (constant number of particles-pressure-temperature) ensembles. In the NPT ensemble, we have applied the Andersen constant pressure method.[38] The cell size in the *z*-direction was chosen so that the slab simulation conditions were fulfilled. A mass for the external system that is required for the simulations[38] was set equal to the mass of all the atoms. When applied to the bulk *a*-SiC, the Andersen scheme gives an equilibrium volume at 300 K that differs by only 0.1% from that obtained from the simulations under constant bulk modulus ($B = 2.2$ Mbar). All the equilibrated samples were relaxed for 5 ps. A time step of 1.0×10^{-15} s is used during all MD simulations. To evaluate the film cohesion we calculated the difference between the potential energies of the samples before and after shifting all the film atoms in the *z*-direction relatively to the substrate by 8.0 Å. The distance of 8.0 Å was sufficient to keep the substrate and the film atoms without interactions.

Along with the calculations of the film structures using the depositionlike technique, we generated a bulk sample of *a*-SiC by cooling the melt, obtained from the 3C-SiC crystal at 8000 K, down to 300 K with a cooling rate of $\sim10^{13}$ K/s. To equilibrate the structures, both the melt and the amorphous sample were let to evolve for 20 ps. The Tersoff potential gives equilibrium lattice parameters of 5.43 and 4.28 Å for *c*-Si and 3C-SiC, respectively, which are rather close to the experimental values of 5.43 and 4.36 Å.[1,2] We considered a lattice parameter of 4.344 Å for the 600-atom bulk sample (*a*-600), as in the case of the as-deposited films. An amorphous bulk originated film (*f*-600) was generated by means of an equilibration of the bulk sample (*a*-600) with two-dimensional periodic boundary conditions during 30 ps at 300 K. The *a*-600 and *f*-600 structures were annealed at 300 K and 2500 K in the NPT ensemble by using both the Andersen and the bulk modulus approaches. The (001) 3C-SiC slab was generated by equilibrating a bulk 512-atom sample with two-dimensional periodic boundary conditions at 300 K during 30 ps in the Andersen NPT ensemble. All the annealed samples under investigation were cooled down to 300 K with an average cooling rate of $\sim10^{13}$ K/s.

Atomic level stresses of annealed *a*-SiC films are evaluated by considering an atomic compression (tension)[39]

$$\sigma_i = -\frac{dE_i}{d\ \ln V} \sim p_i\Omega_i, \tag{1}$$

where E_i is the energy of atom *i* and *V* is the volume. Dividing by the atomic volume, Ω_i, converts σ_i in units of pressure, p_i. The total intrinsic stress of the system can be calculated by summing up σ_i over all atoms. For a completely strain compensated system the total stress is zero. The average atomic volume of the *a*-SiC/*c*-Si systems was considered as the average value between Ω_i of *c*-Si and 3C-SiC structures.

The surface roughness, R_a, of the annealed films is evaluated according to[40]

$$R_a = \sum_i \frac{|Z_i - Z_{\text{ave}}|}{N}. \tag{2}$$

Experimentally, *N* is the number of measured heights during atomic force microscope (AFM) scans, Z_i is a surface height, and Z_{ave} is the average height within a certain area. Within

the simulation cell the surface heights are measured by using a 10×10 uniform grid that corresponds to the conditions of the AFM measurements with a tip size equal to 2.2 Å.

In our investigation, a sp^3s^* TB scheme[41] is used to calculate the DOS of *a*-SiC/*c*-Si samples. Analysis of the local DOS is carried out with the recursion technique of Haydock, Heine, and Kelly,[42] and Nex.[43] The initial cell is duplicated according to the periodic boundary conditions to generate a large cluster of ~5200 atoms. The local DOS of amorphous systems is obtained with 53 levels of continued fraction for the description of the one-electron Green function. This number of levels guarantees a convergence of the DOS for the corresponding crystalline materials.[30,31] The parameters of the sp^3s^* TB scheme for *c*-Si, diamond, and 3C-SiC were carefully determined in Refs. 30, 31, and 44. Therefore, we only note here that our scheme gives BGs of 1.17, 2.40, and 5.50 eV for Si, 3C-SiC, and diamond, respectively, in close agreement with the experimental values. The scaling of the two-center hopping parameters with interatomic distance is chosen according to the Harrison rule.[45]

Following Fedders *et al.*,[46] to clarify the extent of the localization of the electronic states, we define a "localized charge" $q(n,E)$ associated with each eigenvalue with energy E and the atomic site centered on the atom number n. This charge is obtained from the eigenvectors of the TB matrix. The quantity $q(n,E)$ summed over all atoms should be equal to unity, therefore it is not suitable for determining the localization of the electronic states at the energy E. For this reason a mean-square charge is introduced[46]

$$Q(E) = N\sum_n q(n,E)^2, \tag{3}$$

where N is the number of atoms in the sample. Given a distribution $Q(E)$, the localization of a certain state can be evaluated by comparison with the initial charge distribution.

III. RESULTS AND DISCUSSION

A. Atomic configurations and pair correlations

In Fig. 1 we show the atomic configurations of as-deposited *a*-SiC films. The series of the samples was generated depending on the preparation conditions. The following deposition parameters were chosen: T_G=800, 1000, 1200, 1500, and 2000 K; F_N=0.05, 0.08, 0.10, 0.12, 0.15 nN; T_S =300, 600, 800, 1200, and 1500 K. The following abbreviation for the as-deposited films is adopted: $T_G(\times100\text{ K}) - F_N(0.01\text{ nN}) - T_S(\times100\text{ K})$. Hence, a 12-10-06 film is generated at T_G=1200 K, F_N=0.1 nN, and T_S=600 K. One can note in Fig. 1 that the main effect of the increase in the deposition parameters on sample microstructure is displayed in the interface region. It is clearly seen that as the deposition parameters increase, the upper substrate layers undergo an increased distortion that leads to the formation of an amorphous region. The sample densities as functions of the distance along the *z*-direction of the as-deposited and equilibrated samples generated in the NVT ensemble, $N(Z)$, are given in Fig. 2. The results shown in Figs. 1 and 2 clearly indicate that the density of the as-deposited film increases with increasing F_N, while an increase in T_G leads to a decrease in the film density. The change in T_S does not appreciably influence the average film density. For all the films, an increase in the deposition parameters leads to an atomic redistribution from the film surface towards the interface.

The comparison between the densities $N(Z)$ of the as-deposited and equilibrated samples (cf. Fig. 2) shows that the substrate thickness increases after equilibration, which leads to reducing the substrate density. In addition, in the relaxed samples, the amorphous region at the top of the substrate is narrower as compared to that in the as-deposited samples. From these findings we deduce that the substrate in all the as-deposited samples are under compressive stress. As it will be shown below, the as-deposited films are also under compressive stress. Correspondingly, the lattice relaxation caused by sample equilibration reduces the residual compressive stress in both films and substrates.

In Fig. 3 we show the partial pair correlation functions (PCF) in different film and bulk *a*-SiC structures. The structural characteristics of various *a*-SiC samples obtained from MD simulations in the NVT ensemble are presented in Table I. Note that, despite some differences in the structures, the pair correlations in all these systems are very similar. All partial PCF exhibit a distinct peak associated with the nearest neighbor correlations. The main difference between the bulk and film PCF is found in a peak broadening. In the films these peaks are wider than in the bulk. The free surface that gives rise to strongly distorted regions in the films raises the scattering in the first neighbor correlations. Besides, a finite amount of voids in the as-deposited films is revealed, which also promotes the broadening of the pair correlations. The first Si-C peak in the EP bulk sample is higher than in the PA sample. On the other hand, the C-C correlations in the latter sample are more localized than in the former sample. Moreover, the PA C-C peak is located ~0.04 Å lower than the EP C-C peak. This can be explained by the fact that the EP bulk samples have higher chemical ordering and smaller C-C graphitelike bonds than the PA samples (cf. Table I).

Information about the character of the atomic distribution in different amorphous systems can be extracted from the data presented in Table I. The number of fourfold coordinated (T_4) sites is comparable for all bulk samples, with the exception of PA-16 and EP-10000 structures. For the first sample, a "quasiperfect" amorphous structure was generated. The second structure was generated by using the Tersoff potential for C-C interactions determined from graphite.[28] Therefore, in the *a*-SiC samples obtained with involving such a potential, the carbon T_3 configuration is predominant.[25,26,28] From Table I one can see that the percentage of Si-Si and Si-C bonds in all our samples are comparable. However the 12-10-06 films have a larger number of C-C bonds than the *a*-600 and *f*-600 samples. Therefore, when forming *a*-SiC structures, the carbon atoms form diamondlike or graphitelike bonds in the process of the atom-by-atom deposition more efficiently than when cooling from the melt. The increase in the number of threefold coordinated (T_3) atoms in the sequence (*a*-600)-(*f*-600)-(12-10-06) is caused by the appearance of atoms located in the outer and void surfaces. This point will be discussed later.

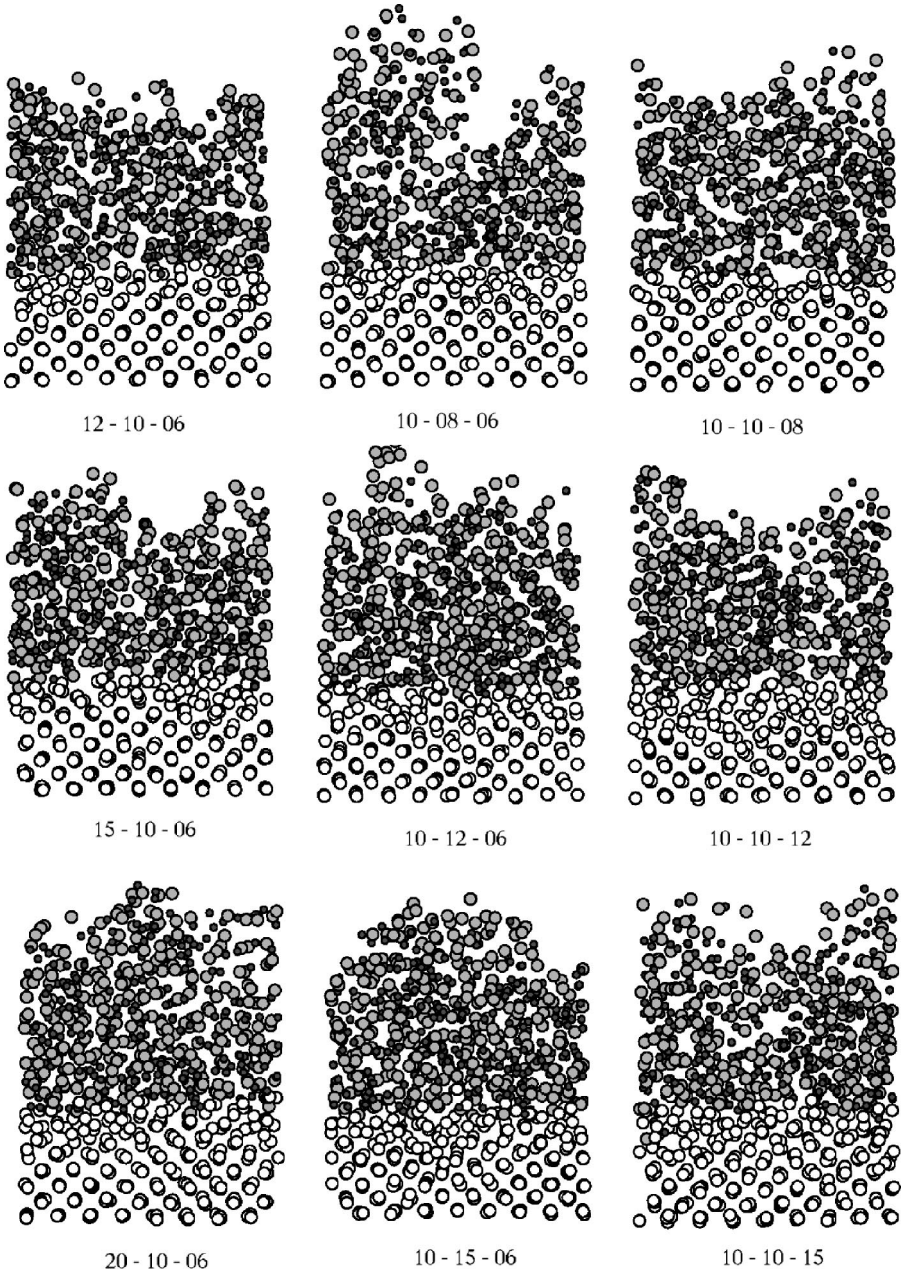

FIG. 1. Projections of atomic arrangements on the *x*-*y* plane of as-deposited *a*-SiC films. For each sample the notations refer to $T_G(\times 100\ \mathrm{K}) - F_N(\times 10^{-2}\ \mathrm{nN}) - T_S(\times 100\ \mathrm{K})$. The full circles correspond to the film Si (large) and C (small) atoms. Only half of the substrate atoms is shown (open large circles).

B. Film characteristics as a function of preparation conditions

Average growth rate (r_D), cohesion energy (E_{Coh}), and number of T_4 atoms (n_4) of the as-deposited and annealed at $T=T_S$ films are shown in Fig. 4 as functions of the deposition parameters. Let us analyze the influence of these parameters on the properties of the theoretical and experimental films. To compare our results with the analogous experimental data we have to find a correspondence between the simulated and experimental deposition parameters. It is difficult to find without ambiguity the experimental counterparts of the model parameters T_G and F_N. However, qualitatively, the gas chamber pressure (P_c) in CVD or the filament temperature (T_f) in hot wire-CVD can be brought in correspondence with the vapor temperature (T_G) defined in our model. We can assume that the negative substrate bias (U_d) that generates the attractive particle force in plasma-CVD corresponds to the normally applied particle force, F_N. As for the correspondence between the theoretical and experimental deposition parameters it should be noted that, for the short simulation time, the Tersoff potential overestimates the melting temperature of crystalline Si and 3C-SiC.[25–27] These values are ~2500 K and ~4000 K, respectively, which are about one and a half times higher than the experimental ones of ~1800 K and ~2900 K, respectively.[1,2,25–27,47] Allowing for this shortcoming of the Tersoff potential, we will analyze below the temperature effects on the samples by comparison.

Figure 4 shows that the increase in T_G and F_N accelerates the film growth process, and inversely, the increase of T_s slows it down. The influence of normally applied forces on deposition rate is appreciably stronger in comparison with other deposition regimes. The effect of substrate temperature at modest values of T_G and F_N on the atomic configuration of the films is to increase the dissipation of the outer atoms,

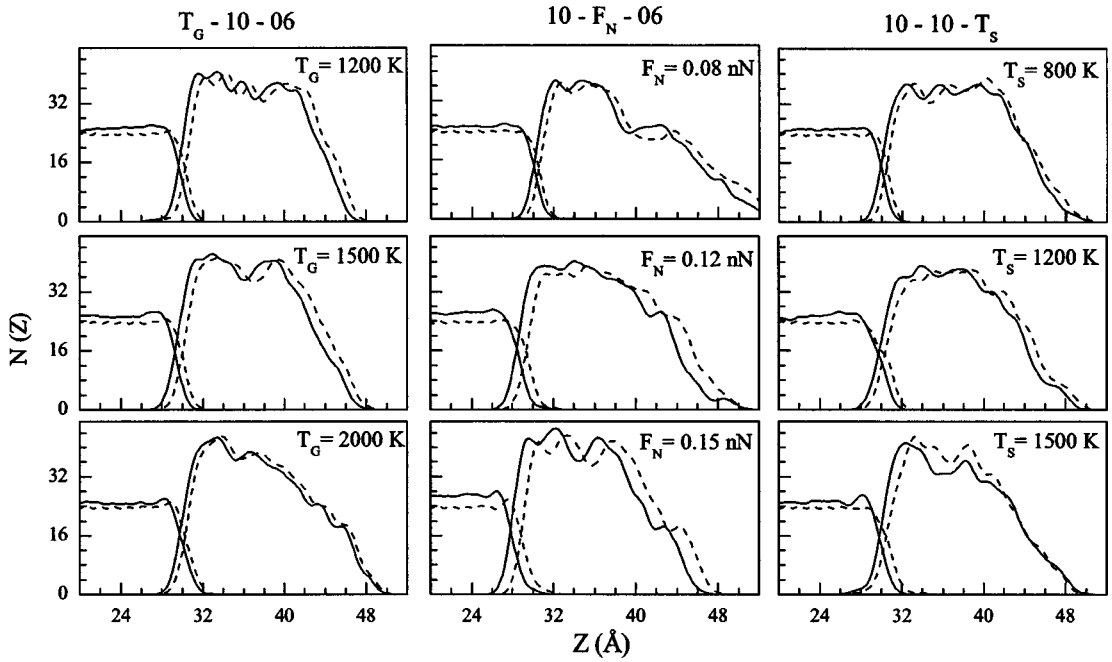

FIG. 2. Densities $N(Z)$ of the as-deposited (solid line) and 600 K annealed samples in the NVT ensemble (dashed line) as functions of distance along the z-direction. The substrate extends up to ~32 Å.

which leads to a decrease in the density in the perturbed region (cf. Fig. 2). Such atomic heat dissipation is enhanced with substrate temperature and prevents film growth. As a result, r_d decreases as T_S increases. This finding is consistent with accepted film growth mechanisms.[7,8,14] An increase in F_N and T_G leads to an accelerated deposition process, regardless of the enhancement of etching reactions, which is consistent with a rise of r_D with an increase of P_c for rf sputtered[14] and photo-CVD,[9] U_d for PECVD (Ref. 8) *a*-SiC and *a*-SiC:H films, and T_f for HW-CVD *a*-SiC:H films.[48] Consequently, for the accepted range of F_N and T_G values, we find that etching is dominated by deposition.

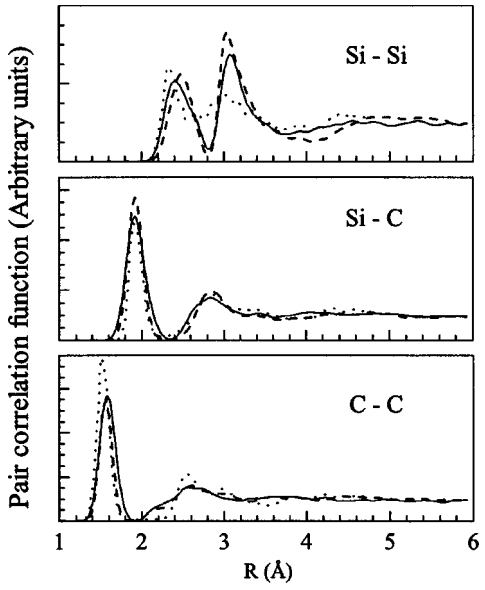

FIG. 3. Partial pair correlation functions of the as-deposited 12-10-06 film (solid line), the 54-atom PA sample (Ref. 21) (dotted line), and the *a*-600 sample (dashed line). All the PCF are normalized to unity around $R=6$ Å.

The adhesion of both the as-deposited and annealed films to the silicon substrate (reflected in the cohesion E_{Coh}) is enhanced as all the deposition parameters increase (cf. Fig. 4). For the as-deposited layers, the influence of normal applied forces is more noticeable, while an increase in substrate temperature only leads to an insignificant increase in film adhesion. The cohesion energy of all films increases upon annealing. The drastic rise in film cohesion with increasing T_S is observed for the equilibrated samples. The film adhesion strengthens during the structural evolution after deposition mostly due to a widening of the interface region. The adhesion of the annealed films deposited at high T_G, F_N, and T_S to the silicon substrate is found to be higher than the cohesion between the substrate layers. We did not find direct experimental evidence for these results on film adhesion. However, the tendency in the variation of the cohesion energy that is established here correlates quite well with an improvement of the mechanical properties of PVD, LAD *a*-SiC,[10,11,13,15] and PECVD *a*-SiC:H (Ref. 49) films with an increase in T_S and T_a. In particular, in the latter case,[49] the *a*-SiC:H coatings deposited on silicon wafers at high temperature exhibit higher abrasive wear resistance compared to the uncovered wafers. The scratch tests[13] have shown that the scratch failure occurs in the silicon substrate and not at the interface for the high temperature PVD *a*-SiC coatings deposited on silicon wafers.

Finally, deviations of the amorphous network from the ideal tetrahedral structure can be evaluated by counting the number n_4 in the *a*-SiC film. The larger n_4 is, the smaller the differences between both structures are. It is well known[1–9] that the deviation from tetrahedral coordination related to

TABLE I. Structural parameters of *a*-SiC bulk and film samples obtained from MD simulations in the NVT ensemble. R_{Si} is the cut-off distance of the Si-Si interactions. In our calculations $R_{C\text{-}C}$ and $R_{Si\text{-}C}$ are equal to 1.9 and 2.2 Å, respectively; n_i is the fraction of *i*-fold coordinated atoms; N_i is the average coordination number of a species *i*; and $N_{i\text{-}j}$ is the fraction of *i*-*j* bonds in the samples.

Sample	R_{Si} (Å)	n_3 (%)	n_4 (%)	n_5 (%)	n_6 (%)	N_{Si}	N_C	$N_{Si\text{-}Si}$ (%)	$N_{Si\text{-}C}$ (%)	$N_{C\text{-}C}$ (%)
PA-54[a]	2.52	17	77	6	0.0	3.93	3.85	23.0	55.0	24.0
PA-16[b]	N/A	0	100	0	0.0	4.00	4.00	7–16	84–68	7–16
EP-512[c]	2.56	N/A	N/A	N/A	N/A	4.39	3.70	29.2	53.5	17.3
EP-10000[d]	N/A	49.8	45.6	4.6	0.0	4.01	3.08	26.1	53.2	20.7
TB-128[e]	2.50	6.3	84.4	9.3	0.0	4.09	3.97	24.0	55.5	22.5
a-600	2.55	10.0	71.2	16.3	1.5	4.15	3.99	18.3	65.4	16.3
	2.60	1.5	67.7	24.0	6.5	4.72	3.99	23.6	61.2	15.2
f-600	2.55	19.7	61.2	13.2	2.3	4.03	3.78	19.6	64.0	16.4
	2.60	16.5	58.3	18.7	4.7	4.40	3.78	23.1	61.2	15.7
12-10-06[f]	2.60	27.6	55.7	8.3	1.0	3.74	3.55	20.1	58.3	21.6
12-10-06[g]	2.60	23.4	62.2	8.3	0.6	3.78	3.69	18.3	61.1	21.6

[a]54- and 16-atom samples are generated by cooling a SiC melt with *ab initio* PA (Refs. 21 and 22).
[b]54- and 16-atom samples are generated by cooling a SiC melt with *ab initio* PA (Refs. 21 and 22).
[c]512-atom sample is generated by cooling the SiC melt with a modified Tersoff potential (Ref. 29).
[d]65000-atom sample is generated by using the fee volume MC method combined with the Tersoff potential (10000 atoms were selected for analyzing) (Ref. 28).
[e]128-atom sample is generated from the SiC vapor with a TB scheme. (Ref. 23).
[f]521-atom as-deposited and annealed at 2000 K films, respectively.
[g]521-atom as-deposited and annealed at 2000 K films, respectively.

various coordination defects leads to a deterioration of optoelectronic properties and to a decrease in phase stability. Figure 4 shows that the number of T_4 atoms steadily increases with an increase in F_N. The variation of n_4 with T_G and T_S of the as-deposited films has a maximum. Correspondingly, the high-quality as-deposited films can be prepared at relatively low temperature and high F_N. In all cases, annealing leads to an increase in n_4. Note that an increase in the substrate temperature can have a positive effect, i.e., can lead to improvement of the amorphous structure provided that the as-deposited films are further equilibrated. Along with the increase in the number of T_4 atoms, chemical ordering and distortions of the tetrahedral configuration are often considered as indicators of network quality.[23–27,29–31] In the *a*-SiC

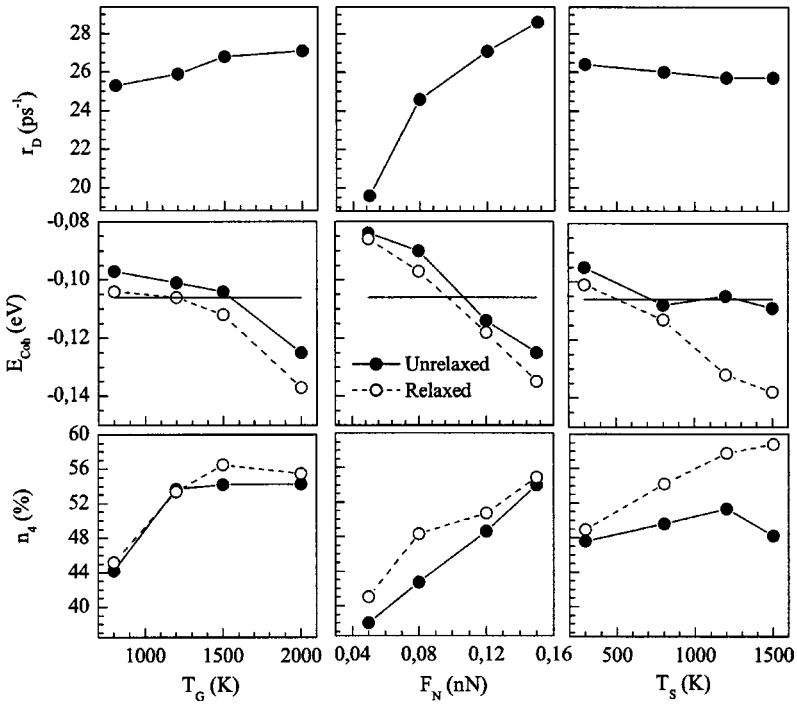

FIG. 4. Average growth rate (r_D), cohesion energy per atom (E_{Coh}), and average number of four-fold coordinated atoms (n_4) of the as-deposited and 600 K annealed films (NVT ensemble) as functions of vapor temperature (T_G), normal force (F_N), and substrate temperature (T_S). The horizontal line in the cohesion energy plot corresponds to the energy needed for separating the substrate into two equal parts along the *z*-direction.

TABLE II. Percentage of $T_3(n_3)$, $T_4(n_4)$ atoms and *i-j* bond ($N_{i\text{-}j}$), cohesion energy per atom (E_{Coh}), surface roughness (R_a), and dimension $a_x=a_y$ of the simulation cell of the as-deposited and annealed 12-10-6 samples generated in the NVT and PVT ensembles.

Annealing temperature	Ensemble	n_3 (%)	n_4 (%)	$N_{\mathrm{Si\text{-}Si}}$ (%)	$N_{\mathrm{Si\text{-}C}}$ (%)	$N_{\mathrm{C\text{-}C}}$ (%)	E_{Coh} (eV)	R_a (Å)	a_x (Å)
	NVT (as-dep.)	27.6	55.7	20.1	58.3	21.6	−0.101	2.60	21.720
600 K	NVT	25.0	55.4	21.2	57.8	21.0	−0.106	2.59	21.720
	NPT	24.8	55.9	21.6	57.4	21.1	−0.110	2.62	21.548
1300 K	NVT	24.8	56.1	21.3	58.0	20.7	−0.122	2.36	21.720
	NPT	22.6	58.7	20.0	59.4	20.6	−0.122	2.49	21.394
2000 K	NVT	23.4	62.2	18.3	60.1	21.6	−0.144	2.19	21.720
	NPT	21.7	63.5	18.8	60.2	21.0	−0.126	2.23	21.422
2500 K	NVT	20.7	63.2	18.0	61.1	20.9	−0.186	1.94	21.720
	NPT	19.4	64.3	18.1	61.8	20.1	−0.164	1.99	21.403

films chemical ordering is found to be weakly sensitive to the selected preparation conditions. The percentage of hetero-nuclear bonds averages $59\pm2\%$. A number of hetero-nuclear bonds slightly increase upon equilibrating, on average, by $1-2\%$. The increase in n_4 and heteronuclear bonding with an increase in T_S is consistent with *a*-SiC getting more similar to the crystal-like tetrahedral structure,[1,2,50–56] at high deposition temperature. For LAD *a*-SiC films, as T_S is raised, the optical BG increases along with a reduction in the density of paramagnetic defects,[23–27,29–31] which points to a decrease in the number of abnormally coordinated sites.

C. Structural relaxation under annealing

To clarify the nature of the structural transformation in *a*-SiC films under annealing conditions we investigated in detail the atomic configuration and atomic stress state of the 12-10-06 sample annealed at 600, 1300, 2000, and 2500 K in the NVT and NPT ensembles. Table II contains the structures parameters of the annealed samples. Without entering the details, note that all the structural parameters of the NVT and NPT films vary similarly with annealing temperature. However, a closer inspection shows that the number of hetero-nuclear bonds in the latter films is larger as compared with that in the NVT structures. Correspondingly, a free volume change in the NPT systems enhances lattice relaxation that promotes a form of hetero nuclear bonds. An increase in annealing temperature leads to a noticeable increase in the number of T_4 atoms and heteronuclear bonds. The C-C network is weakly changed with annealing temperature, and this can be attributed to the higher strength of the C-C bond energy compared to the energy of the Si-Si and Si-C interactions. This bond redistribution is clearly reflected in Fig. 5, where the theoretical and experimental pair correlation functions of the as-deposited and annealed films are displayed. One can see that the changes in the experimentally measured reduced radial distribution function when going from as-irradiated to 800 °C annealed *a*-SiC (Ref. 19) are similar to those in the calculated spectrum upon annealing.

Although we did not find any direct information on an effect of annealing on cohesion properties of *a*-SiC films, we believe that such information deduced from our theoretical experiment will be useful when interpreting the tribological properties of coatings based on *a*-SiC as was discussed above. As seen from Table II, the cohesion of *a*-SiC film to silicon substrate rises with an increase in the annealing temperature. To understand this cohesion enhancement, one can analyze the density profile of the annealed samples along the *z*-direction, as shown in Fig. 6. We will assume that an increase in film cohesion with T_a occurs because of a widening of the interface region, which is related to spreading the substrate atoms into the film layers. The latter leads to increasing the number of the carbon atoms and Si-C bonds at the interface. As a result, the substrate-film cohesion becomes stronger than the energy needed for separating the substrate

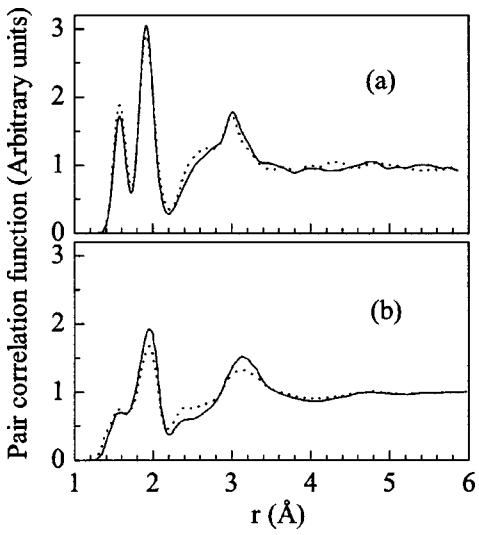

FIG. 5. Pair correlation function of (a) the 12-10-06 film annealed at 600 K (dashed line) and at 2500 K (solid line); and (b) the as-irradiated (dashed line) and 800 °C annealed (solid line) *a*-SiC layers (Ref. 19). The theoretical samples were generated in the NPT ensemble.

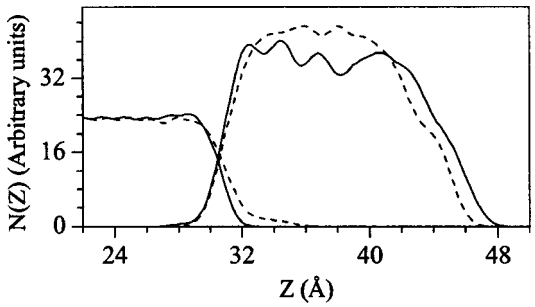

FIG. 6. Density $N(Z)$ of the 12-10-06 samples annealed at 600 K (solid line) and at 2500 K (dashed line) in the NPT ensemble as a function of distance along the z-direction.

layers already for $T_a > 600$ K. Upon annealing, along with the interface broadening, the voids at the interface are annealed. Consequently the interface becomes denser, and the film adhesion is enhanced.

We evaluated the surface roughness of the annealed films as a function of T_a. This value is reduced with increasing T_a (cf. Table II). Taking into account the density profile (see Fig. 6) and the values of a_x summarized in Table II, one can see that the films become more homogeneous and denser with an increase in T_a, which is mostly associated with the atomic relaxation around microvoids. In Fig. 7 we show the atomic configuration in the x-y plane for a series of annealed samples. One such void can be observed at the center of the as-deposited 12-10-06 film. The void spreads from the outer surface down to the substrate. An increase in T_a promotes atomic relaxation around the void, which leads to a decrease in the void volume and, when T_a is raised further, to its disappearance accompanied by an increase in the film density and a reduction of the surface roughness. Here, it should be pointed out that an increase in T_a from 600 K to 2500 K leads to a reduction in density of the a-600 and f-600 samples by 2.8% and 3.8%, respectively. This finding prompts us to conclude that the observed increase in film density with rising annealing temperature is mainly due to the disappearance of voids. This conclusion is in agreement with the experimental observations.[57] Indeed, Höfgen *et al.*[57] examined the annealing behavior of a-SiC using profilometry and x-ray diffraction, and observed large volume reduction of a-SiC prior to crystallization. A previous investigation reported that the annihilation of point defects leads to substantial densification.[58]

Additional information about atomic configuration in a-SiC films can be obtained from the bond-angle distribution

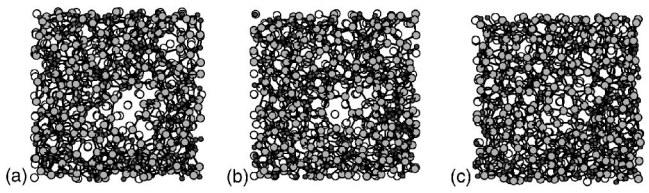

FIG. 7. Atomic configurations in the x-y plane of the (a) as-deposited, (b) annealed at 2000 K, and (c) annealed at 2500 K 12-10-06 samples in the NPT ensemble (notations similar to those given in Fig. 1).

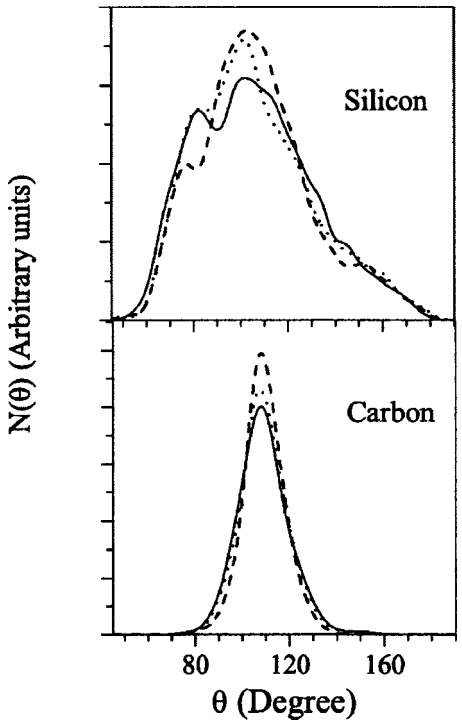

FIG. 8. Bond-angle distribution $N(\theta)$ of the as-deposited (solid line) and annealed at 1300 K (dotted line) and 2500 K (dashed line) 12-10-06 film in the NPT ensemble.

functions, $N(\theta)$, shown in Fig. 8. If an amorphous structure contains an appreciable number of T_3, T_4, and T_5 atoms, its bond-angle distribution should have three peaklike features related to these groups of abnormally coordinated atoms at approximately 120°, 109°, and 80–90°, respectively. These peculiarities are indeed present in $N(\theta)$ of silicon atoms. Taking into account the fact that the main peak of the silicon $N(\theta)$ function is located around 109°, one can say that the silicon configuration in a-SiC films represents a strongly distorted tetrahedral network. This finding is consistent with the results of extended x-ray absorption fine structure investigations[59] and with the theoretical results for the melt-derived bulk a-SiC.[21,27,28] Annealing leads to an enhancement of the tetrahedral bond angle of 109°, which is consistent with an increase of T_4 sites with an increase in annealing temperature, as stated earlier. Another picture of the bond-angle distribution is observed for carbon atoms. We see that the carbon $N(\theta)$ function has one distinct peak around the tetrahedral bond angle. This peak becomes more prominent in the annealed samples. Hence, the carbon atoms form a tetrahedral network that is less distorted compared to that formed by silicon atoms. Since the tail of the peak overlaps the bond-angles around 120°, one can conclude that the carbon atoms along with T_4 configurations form T_3 ones. About 30% of all carbon T_3 atoms were found to be clean graphite like sp^2 sites. So, the bond-angle distributions in a-SiC films clearly show that, during annealing, both the Si and C local geometries are transformed in such a way that an enhancement of the tetrahedral configurations in the amorphous network is favored.

Let us now consider the atomic level stresses, which are a measure of the rigidity of the network of a-SiC films. It is

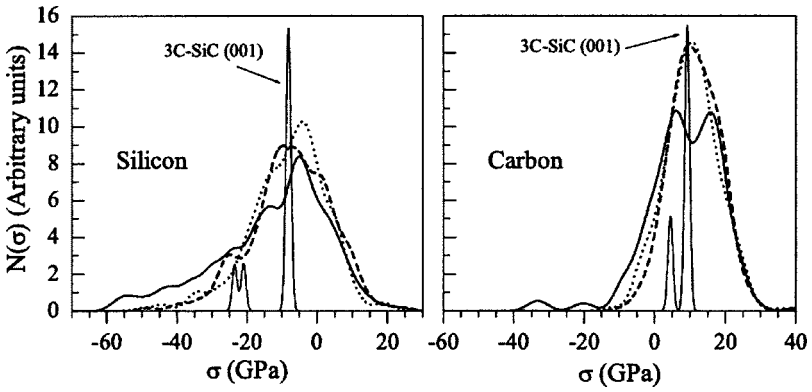

FIG. 9. Atomic stress distribution $N(\sigma)$ of the as-deposited (solid line) and annealed at 600 K (dotted line) and 2000 K (dashed line) 12-10-06 sample in the NPT ensemble. Edge smearing of the stress distribution of the 512-atom 3C -SiC(001) slab was reduced to single out stress localization.

well known that the local stresses are present in networks with non-equivalent atoms and in any disordered structure. In Fig. 9 we show the distributions of atomic stresses $N(\sigma)$ for the as-deposited and annealed 12-10-06 films. For the sake of comparison, we also present the function $N(\sigma)$ for the (001) 3C-SiC slab. The Si and C atoms in a 512-atom crystalline bulk sample were found to be under compressive and tensile stresses of about 8.7 GPa, respectively. In the case of a 512-atom (001) slab, the surface Si and C atoms are located closer to the bulk by approximately 5% and 0.3%, respectively, as compared with the Si-C interlayer distance in the corresponding bulk sample. These structural peculiarities of the crystalline slab are reflected in the stress distributions. The Si projected $N(\sigma)$ has one main peak at around −8.1 GPa related to the bulk atoms and two minor peaks at −23.5 GPa and −21.0 GPa associated with the surface and undersurface Si atoms, respectively. The C function $N(\sigma)$ has one main peak located at around 9.1 GPa that is related to the atoms inside the slab, and one minor peak at approximately 4.5 GPa associated with the surface and undersurface atoms. In the amorphous samples the functions $N(\sigma)$ are widespread, indicating the presence of large internal local stresses, compressive as well as tensile for both types of atoms (cf. Fig. 9). The tails of the distributions originate from atoms having severely strained bonds and angles, and which are weakly bonded. Since the amorphous network of Si atoms is more strongly distorted than the C network, the distribution $N(\sigma)$ related to Si atoms is broader than the analogous distribution for C atoms. However, despite the widespread structure of the stress distributions, the main peak of the Si function $N(\sigma)$ is located in a compressive stress region (around −10 GPa), while two main peaks of the C function $N(\sigma)$ observed around 4 GPa and 16 GPa are located in the tensile stress region. Upon annealing the main peaks in both stress distributions approach those observed in the stress distributions of the crystalline slab. We found that the average film stress varies from −1.8 to 2.2 GPa when going from the as-deposited to annealed at the 2000 K sample. The Si atoms belonging to the substrate in the as-deposited sample give rise to one distinct peak in $N(\sigma)$ around −8.9 GPa (not shown in Fig. 9), which upon annealing at 2000 K becomes narrower and shifts to a new position at −1.7 GPa. Therefore, sample annealing leads to a reduction of the compressive stress of the Si substrate and to a modification of the nature of the average film stress from compressive to tensile. The latter conclusion is confirmed experimentally by the increase in the tensile stress of PECVD *a*-SiC:H films deposited on crystalline silicon wafers with an increase in annealing temperature from 600 to 900 °C.[60,61] Such a comparison is allowed, since in this temperature region the films remain amorphous and practically do not contain bonded hydrogen.[61] Considering the fact that 3C-SiC can be epitaxially grown on a silicon substrate at comparatively high deposition temperatures and that the interface region contains dislocations[2,62] together with our results, one can suppose that the tensile stress of the annealed films is related to the mismatch between *c*-Si and 3C-SiC lattices (about 20%), and to the difference in thermal expansion coefficients (about 8%).

D. Electronic states and their localization

Typical layer-projected TB-DOS associated with atoms located in the middle of the substrate, at the interface and in the middle of the 12-10-06 sample are displayed in Fig. 10. The spectra were calculated using the final atomic configurations determined from EP-MD simulations. The substrate DOS shows a distinct band gap around 0.0 eV [Fig. 10(a)]. Although the interface and film DOS exhibit a trend toward band gap formation around 0.0 eV, a significant amount of deep states are present in the band gap region [Figs. 10(b) and 10(c)]. It is well known that gap states are caused by coordination defects, strongly distorted T_4 sites, and homonuclear bonds.[30,31] All these defects are present in both the interface and the film regions. The interface DOS is separated by the contributions from the substrate Si atoms [Fig. 10(b)], the film Si and C atoms [Fig. 10(c)]. It is seen from Fig. 10 that the electronic spectrum (b) is closer to the bulk DOS (a) than the Si projected partial DOS (c). It follows that the Si film atoms are distributed at the interface more randomly than the Si atoms belonging to the substrate. The pseudoband gap around 0.0 eV becomes wider when going from the interface to the middle of the film, and this can be attributed to an increase in the number of C atoms in the nearest neighbor shells surrounding the Si atoms. The band-gap broadening is accompanied by the disappearance of the peak around −1.0 eV in the C projected DOS. This peak is assigned to C sp and sp^2 states.[23,24] From this we deduce that the number of abnormally coordinated C atoms in the interface region is larger compared to that inside the film.

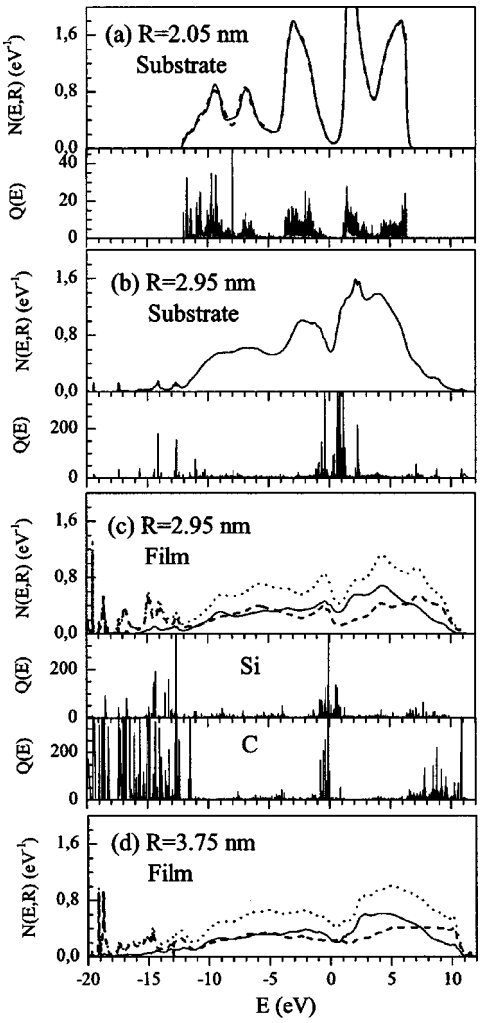

FIG. 10. Local layer-projected DOS $N(E,R)$ associated with (a) the middle of the substrate—$N(E)$ obtained using a 1289 (solid line) and 5156 (dashed line)—atom cell; (b and c) the interface, and (d) the middle of the as-deposited 12-10-06 film: Si-projected DOS (solid line), C-projected DOS (dashed line) and total DOS (dotted line). R is the distance relative to the bottom of the substrate (see Fig. 2). Mean-square charge distribution $Q(E)$ related to the (a) substrate DOS, and (b and c) and the interface DOS. The Fermi energy is located around 0.170 eV.

An important characteristic of the DOS is the extent of the electronic localization $Q(E)$ over the range of the electronic spectrum. We see that, for the almost perfect electronic spectrum inside the substrate, electronic states are weakly localized at the band edges [Fig. 10(a)]. In the case of the substrate atoms at the interface, the strong electronic localization takes place at the bottom and at the top of the band gap [Fig. 10(b)]. The states originated from the Si film atoms at the interface are localized mostly at midgap and at the bottom of the valence band [Fig. 10(c)]. The carbon atoms located in the interface region give rise to strong electronic localization at the bottom of the valence band, in the band gap, and at the top of the valence band [Fig. 10(c)]. We found a similar distribution of localized states for atoms located in the middle of the film (not shown). It follows that, regardless of the presence of a significant amount of gap states (that are

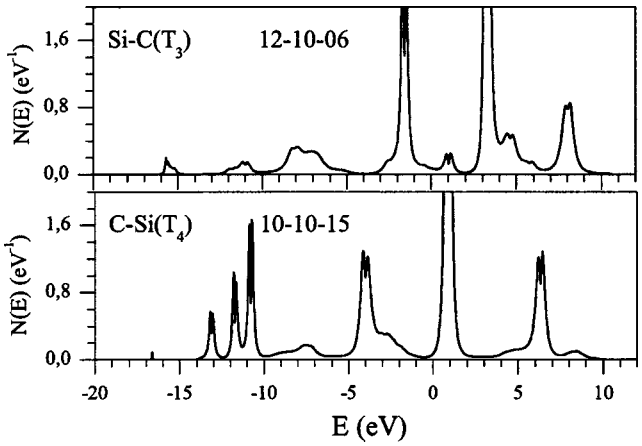

FIG. 11. Local DOS $N(E)$ associated with singlefold coordinated Si and C atoms located on the outer surface of the as-deposited samples.

associated with the interface and middle film regions) in the DOS, the film will exhibit semiconductor properties, since these states are strongly localized (correspondingly, they will not contribute to conductivity). On the other hand, they act as traps for carriers. To improve the optoelectronic properties of the films, deposition should be carried out from silicon and carbon containing precursors in the presence of hydrogen.[1–9]

As far as the semiconductor properties of *a*-SiC films are concerned, we note that, so far, the role of the surface atoms in *a*-SiC films in generating gap states has not yet fully clarified. By analogy with the hydrogen effect on dangling-bond states one would expect that the surface singlefold coordinated silicon or carbon atoms will be able to make the weak-bond passivation and will not give rise to gap states. As was mentioned above, the influence of other abnormally coordinated sites on the electronic spectrum was thoroughly examined earlier.[23,24,30,31] Here, we present the results of the calculations of the local DOS associated with the singlefold coordinated Si and C atoms located on the outer film surface. In Fig. 11 we report the local DOS of such atoms belonging to as-deposited *a*-SiC films. It is seen that, in contrast with the expected results, both types of atoms give rise to gap states. The local DOS of the silicon atom in the Si-C(3) configuration and the carbon atom in *C*-Si(4) configuration exhibit distinct deep levels at the top of the band gap. Gap states having the C-origin are more localized than those caused by the Si atom in the single fold coordinated configuration. A similar situation is observed for T_3 atoms (not shown). We expect that such circumstance is responsible for the single EPR signal with a g value of 2.0028 associated with the abnormally coordinated C atoms detected by Tabbal *et al.* in *a*-SiC films.[16,17]

As was mentioned above, an increase in the Si-C heteronuclear bond density and some local ordering caused by annealing lead to an improvement of the optoelectronic properties, and to a widening of the band gap in *a*-SiC films.[16,17,54] The observed variations of the electronic spectra of as-deposited *a*-SiC films under annealing shown in Fig. 12 are consistent with this tendency. Upon annealing, the dip in

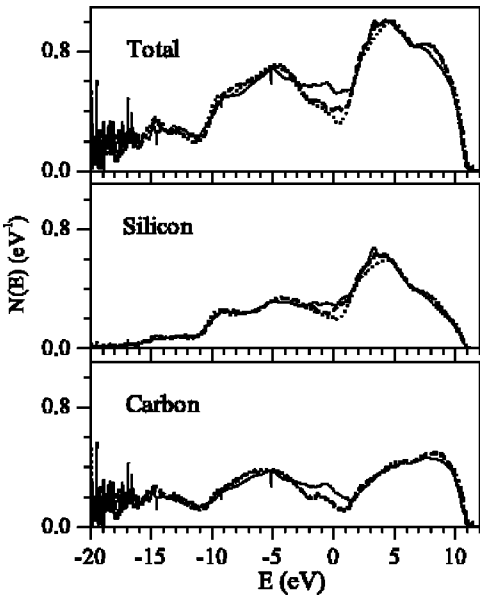

FIG. 12. Densities of states $N(E)$ of the as-deposited (solid line), annealed at 2000 K (dashed line) and 2500 K (dotted line) 12-10-06 samples in the NPT ensemble.

the band gap region becomes deeper, and this is attributed to an improvement of the amorphous tetrahedral network. The band gap in the silicon projected DOS is formed in a narrow region around 0.0 eV, mostly due to a reduction of the Si dangling and homonuclear bonds. A change of the atomic configurations around the C atoms during annealing leads to the formation of a band gap in a wide energetic range. The peak around −1.0 eV in the carbon projected DOS, associated with *sp*- and sp^2-configurations, is reduced during annealing. Here, it should be noted that, in contrast to first-principles procedures, the Tersoff potential tends to overestimate a number of T_3 atoms located at the sample surface.[63] So one can expect that our approach provides more gap states than first-principles methods.

IV. CONCLUSIONS

We have investigated the atomic and electronic structures and growth kinetics of *a*-SiC films. For this purpose a deposition scheme based on empirical molecular dynamics simulations was suggested. A set of films was generated by condensing the SiC vapor on a (001) silicon substrate as a function of vapor temperature, normally applied particle forces, and substrate temperatures. The as-deposited films were further annealed. The films exhibit pair correlations that are similar to those for bulk *a*-SiC. We find that an increase in vapor temperature and applied forces leads to an increase in the deposition rate, film cohesion, and the improvement of the amorphous network. An increase in substrate temperature slows down the deposition and enhances film adhesion. Sample annealing enhances the film adhesion, and improves the tetrahedral network and, to a lesser extent, chemical ordering, by reducing the number of Si-Si homonuclear bonds. The compressive stress of the silicon substrate is significantly reduced upon annealing, and the average film stress changes from compressive to tensile. The local densities of electronic states related to the interface atoms and to the film atoms exhibit a tendency towards band-gap formation. The localization of the electronic states is highest in the band-gap region and at the band edges. Upon annealing the semiconductor dip increases, and this is mostly attributed to a reduction in Si-Si homonuclear and C *sp*- and sp^2-configurations. The comparison between the computed characteristics and the analogous theoretical and experimental findings for bulk and film *a*-SiC and *a*-SiC:H samples validates our approach.

ACKNOWLEDGMENTS

This work was supported in part by STCU Contract No. 1590-C, 1591. The work of P. E. A. T. was performed under the auspices of U. S. Department of Energy by the University of California Lawrence Livermore National Laboratory under Contract No. W-7405-ENG-48.

[1] J. Bullot and M. P. Schmidt, Phys. Status Solidi B **143**, 345 (1987).
[2] *Amorphous and Crystalline Silicon Carbide: Materials and Applications*, Proc. E-MRS, edited by L. Calcagno, A. Hallen, R. Martins, and W. Skorupa (Elsevier, Amsterdam, 2001).
[3] D. Kruangam, T. Endo, M. Deguchi, W. Guang-Pu, H. Okamoto, and Y. Hamakawa, Opto-electronics (London) **1**, 67 (1986).
[4] Y. Hamakawa, Renewable Energy **15**, 22 (1998).
[5] A. Desalvo, F. Giorgis, C. F. Pirri, E. Tresso, P. Rava, A. Galloni, R. Rizolli, and C. Summonte, J. Appl. Phys. **81**, 7973 (1997).
[6] G. Ambrosone, V. Ballarini, U. Coscia, S. Ferrero, F. Giorgis, P. Maddalena, A. Patelli, P. Rava, and V. Rigato, Thin Solid Films **427**, 279 (2003).
[7] J.-H. Park, H.-S. Kwon, and J.-Y. Lee, J. Appl. Phys. **72**, 5246 (1992).
[8] M. M. Rahman, C. Y. Yang, D. Sugiarto, A. S. Byrne, M. Ju. K. Tran, K. H. Lui, T. Asano, and W. F. Stickle, J. Appl. Phys. **67**, 7065 (1990).
[9] S. Ghosh, A. De, and S. Ray, Thin Solid Films **245**, 249 (1994).
[10] M. E. El Khakani, M. Chaker, A. Jean, S. Boily, J. C. Kieffer, M. E. O'Hern, M. F. Ravet, and F. Rousseaux, J. Mater. Res. **9**, 96 (1994).
[11] M. A. El Khakani, M. Chaker, M. E. O'Hern, and W. C. Oliver, J. Appl. Phys. **82**, 4310 (1997).
[12] B. Cros, E. Gat, and J. M. Saurel, J. Non-Cryst. Solids **209**, 273 (1997).
[13] J. Esteve, A. Lousa, E. Martinez, H. Huck, E. B. Halac, and M. Reinoso, Diamond Relat. Mater. **10**, 1053 (2001).
[14] W. K. Choi, F. L. Loo, C. H. Ling, F. C. Loh, and K. L. Tan, J. Appl. Phys. **78**, 7289 (1995).
[15] H. Kung, T. R. Jervis, J. P. Hirvonen, J. D. Embury, T. E. Mitchell, and M. Nastasi, Philos. Mag. A **71**, 759 (1995).

[16] M. Tabbal, S. Isber, T. C. Christidis, M. A. El Khakani, and M. Chaker, J. Appl. Phys. **88**, 5127 (2000).
[17] T. Christidis, M. Tabbal, S. Isber, M. A. El Khakani, and M. Chaker, Appl. Surf. Sci. **184**, 268 (2001).
[18] S. Ghosh, P. Bhattacharya, and D. N. Bose, Appl. Phys. Lett. **68**, 2979 (1996).
[19] M. Ishumaru, In-Tae Bae, Y. Hirotsu, S. Matsumura, and K. Sickafus, Phys. Rev. Lett. **89**, 055502 (2002).
[20] S. Muto and T. Tanabe, J. Appl. Phys. **93**, 3765 (2003).
[21] F. Finocchi, G. Galli, M. Parrinello, and C. M. Bertoni, Phys. Rev. Lett. **68**, 3044 (1992).
[22] P. C. Kelires and P. J. H. Denteneer, Solid State Commun. **87**, 851 (1993).
[23] V. I. Ivashchenko, P. E. A. Turchi, V. I. Shevchenko, L. A. Ivashchenko, and G. V. Rusakov, Phys. Rev. B **66**, 195201 (2002).
[24] V. I. Ivashchenko, P. E. A. Turchi, V. I. Shevchenko, L. A. Ivashchenko, and G. V. Rusakov, Diamond Relat. Mater. **12**, 993 (2003).
[25] P. C. Kelires, Europhys. Lett. **14**, 43 (1991).
[26] P. C. Kelires, Phys. Rev. B **46**, 10 048 (1992).
[27] J. Tersoff, Phys. Rev. B **49**, 16 349 (1994).
[28] C. R. S. da Silva, J. F. Justo, and A. Fazzio, Phys. Rev. B **65**, 104108 (2002).
[29] D. Mura, L. Colombo, R. Bertoncini, and G. Mula, Phys. Rev. B **58**, 10 357 (1998).
[30] V. I. Ivashchenko and V. I. Shevchenko, Appl. Surf. Sci. **184**, 137 (2001).
[31] V. I. Ivashchenko, V. I. Shevchenko, G. V. Rusakov, A. S. Klymenko, V. M. Popov, L. A. Ivashchenko, and E. I. Bogdanov, J. Phys.: Condens. Matter **14**, 1799 (2002).
[32] F. Finocchi and G. Galli, Phys. Rev. B **50**, 7393 (1994).
[33] V. I. Ivashchenko, P. E. A. Turchi, V. I. Shevchenko, L. A. Ivashchenko, and G. V. Rusakov, J. Phys.: Condens. Matter **15**, 4119 (2003).
[34] F. Gao and W. J. Weber, Phys. Rev. B **63**, 054101 (2000).
[35] F. Gao and W. J. Weber, J. Appl. Phys. **89**, 4275 (2001).
[36] F. Gao, W. J. Weber, and W. Jiang, Phys. Rev. B **63**, 214106 (2001).
[37] J. M. Perlado, L. Malerba, and T. Diaz de la Rubia, Mater. Res. Soc. Symp. Proc. **540**, 171 (1999).
[38] H. C. Andersen, J. Phys. Chem. **72**, 2384 (1980).
[39] P. Kelires, Phys. Rev. Lett. **73**, 2460 (1994).
[40] R. Haerle, A. Baldereschi, and G. Galli, J. Non-Cryst. Solids **266-269**, 740 (2000).
[41] P. Vogl, H. P. Hjalmarson, and J. D. Dow, J. Phys. Chem. Solids **44**, 365 (1983).
[42] R. Haydock, V. Heine, and M. J. Kelly, J. Phys. C **5**, 2845 (1972).
[43] C. M. M. Nex, Comput. Phys. Commun. **34**, 101 (1984).
[44] J. Robertson, Philos. Mag. B **66**, 615 (1992).
[45] W. A. Harrison, *Electronic Properties of Solids* (Freeman, San Fransisco, 1980).
[46] P. A. Fedders and D. A. Drabold, Phys. Rev. B **47**, 13 277 (1993).
[47] *Amorphous and Crystalline Silicon Carbide and Related Materials*, edited by G. L. Harris and C. Y. Yang (Springer Verlag, New York, 1989).
[48] I. Ferreira, E. Fortunato, and R. Martins, Thin Solid Films **427**, 231 (2003).
[49] O. K. Porada, V. I. Ivashchenko, L. A. Ivashchenko, G. V. Rusakov, and S. M. Dub, Surf. Coat. Technol. **180-181**, 122 (2004).
[50] L. Calcagno, P. Musumeci, F. Roccaforte, C. Bongiorno, and G. Foti, Appl. Surf. Sci. **184**, 123 (2001).
[51] L. Calcagno, P. Musumeci, R. Roccaforte, C. Bongiorno, and G. Foti, Thin Solid Films **431**, 298 (2002).
[52] M. B. Yu, Rusli, S. F. Yoon, Z. M. Chen, J. Ahn, Q. Zhang, K. Chew, and J. Cui, J. Appl. Phys. **87**, 8155 (2000).
[53] F. Demichelis, C. F. Pirri, and E. Tresso, Philos. Mag. B **66**, 135 (1992).
[54] Y. Matsumoto, G. Hirata, H. Takakura, H. Okamoto, and Y. Hamakawa, J. Appl. Phys. **67**, 6538 (1990).
[55] S. J. Toal, H. S. Reehal, N. P. Barradas, and C. Jeynes, Appl. Surf. Sci. **138-139**, 424 (1999).
[56] W. K. Choi, T. Y. Ong, L. J. Han, F. C. Loh, and K. L. Tan, Phys. Status Solidi A **169**, 67 (1998).
[57] A. Hofgen, V. Heera, F. Eichhorn, and W. Skorupa, J. Appl. Phys. **84**, 4769 (1998).
[58] V. Heera, F. Prokert, N. Schell, H. Seifarth, W. Fukarek, M. Voelskow, and W. Skorupa, Appl. Phys. Lett. **70**, 3531 (1997).
[59] W. Bolse, J. Conrad, F. Harbsmeier, M. Borowski, and T. Rodle, Mater. Res. Soc. Symp. Proc. **248-249**, 319 (1997).
[60] U. Schmid, M. Eickhoff, Ch. Richter, G. Krotz, and D. Schmitt-Landsiedel, Sens. Actuators, A **94**, 87 (2001).
[61] M. A. El Khakani, M. Chaker, A. Jean, S. Boily, H. Pepin, J. C. Kieffer, and S. C. Gujrathi, J. Appl. Phys. **74**, 2834 (1993).
[62] C. Long, S. A. Ustin, and W. Ho, J. Appl. Phys. **86**, 2509 (1999).
[63] G. Hadjisavvas, G. Kopidakis, and P. C. Kelires, Phys. Rev. B **64**, 125413 (2001).